Gap states due to stretched bonds at the (112) Σ3 boundary in diamond

2007 J. Phys.: Condens. Matter 19 026223

(http://iopscience.iop.org/0953-8984/19/2/026223)

INSTITUTE OF PHYSICS PUBLISHING JOURNAL OF PHYSICS: CONDENSED MATTER

J. Phys.: Condens. Matter **19** (2007) 026223 (9pp) doi:10.1088/0953-8984/19/2/026223

Gap states due to stretched bonds at the (112) Σ3 boundary in diamond

Hidetaka Sawada[1,3], **Hideki Ichinose**[1] **and Masanori Kohyama**[2]

[1] Department of Materials Science, The University of Tokyo, 7-3-1 Hongo, Bunkyo-ku, Tokyo 113-8656, Japan
[2] Research Institute for Ubiquitous Energy Devices, National Institute of Advanced Industrial Science and Technology, 1-8-31 Midorigaoka, Ikeda, Osaka 563-8577, Japan

E-mail: hsawada@jeol.co.jp

Received 29 July 2006, in final form 27 November 2006
Published 15 December 2006
Online at stacks.iop.org/JPhysCM/19/026223

Abstract

The atomic and electronic structure of the $(\bar{1}12)$ Σ3 boundary in diamond has been examined using the density-functional theory with the plane-wave pseudopotential method. Boundary states lower than the bulk conduction-band minimum have been observed in the reconstructed structure without rigid-body translation (RBT), consistent with recent high-resolution transmission electron microscopy observations. These gap states are attributed to the weak reconstructed bonds largely stretched along [110]. It is concluded that the experimentally observed small line below the σ^* line in electron energy loss spectroscopy of this boundary corresponds to the gap states of the stretched bonds. The origins of the appearance of the structure without RBT in spite of its high energy in diamond are discussed.

1. Introduction

It is necessary for us to analyse the atomic and electronic structure of planar defects in a chemical vapour deposited (CVD) diamond film using high-resolution transmission electron microscopy (HRTEM) [1] and electron energy-loss spectroscopy (EELS) [2] because the lattice imperfection in a diamond film prevents us from using the remarkable physical and chemical properties of diamond, such as high thermal conductivity, extreme hardness, high Young's modulus, high melting point, negative electron affinity, high electron and hole mobility and so on [3]. Our previous reports revealed that the grain boundary structure in diamond has characteristic features, being different from other covalently bonded materials such as Si and Ge even though these materials share the common atomic structure of Σ3 and Σ9 coincident-site-lattice (CSL) grain boundaries [1, 2].

[3] Present address: Electron Optics Division, JEOL Ltd, 3-1-2 Musashino, Akishima, Tokyo 196-8558, Japan.

The {112} Σ3 boundary is one of the dominant CSL boundaries commonly observed in CVD films of covalent materials. In diamond, the structure without rigid-body translation (RBT) across the $(\bar{1}12)$ boundary plane is dominant for the $(\bar{1}12)$ Σ3 boundary [1, 2], while the structure with a RBT along the $[\bar{1}1\bar{1}]$ and $[\bar{1}12]$ directions across the $(\bar{1}12)$ boundary planes is dominant in Si and Ge [4, 5]. The EELS spectra of the {112} Σ3 grain boundary shows a EELS line corresponding to a 1s $\rightarrow$ π^* transition below the σ^* line [2], while the {221} Σ9 and {111} Σ3 boundaries do not show such peaks. The presence of this π^* line indicates that unoccupied gap states should exist in particular CSL boundaries such as the {112} Σ3 boundary, in contradiction to the previously accepted knowledge about CSL boundaries in Si and Ge which have no gap states theoretically or experimentally [5, 6]. Thus the atomic and electronic structure of the {112} Σ3 boundary in diamond is quite interesting. There is as yet no clear explanation for the dominant population of the structure without the RBT and the gap states for the diamond {112} Σ3 boundary, although tight-binding calculations have been performed [7, 8]. In this study, therefore, we use the first-principles method based on the density-functional theory [9, 10] for its high precision in analysing the atomic and electronic structure. We calculate the stable configuration and electronic structure of the {112} Σ3 boundary in diamond based on the atomic models [11, 12] given by atomic resolution high-voltage electron microscopy (ARHVTEM) [13].

2. Method

We employed the plane-wave pseudopotential method [14, 15] based on the density-functional theory with the local density approximation [16]. Troullier–Martins optimized pseudopotentials [17] for carbon were constructed with the configuration of $2s^2 2p^2$ and cut-off radii of 1.44 au. The conjugate-gradient method [18, 19] was used for the electronic minimization. The calculated equilibrium lattice constant of diamond crystal is 99.1% (0.3535 nm) of the experimental value. The band gap was calculated using the unit cell. The calculated (indirect) band gap was 4.548 eV (the direct band gap was 5.645 eV).

The initial atomic structure for the relaxation was determined from the micrograph [11, 12]. Super-cells with 48 and 96 atoms are used for the (1 × 1) and (1 × 2) models, respectively, as explained below. The periodicity in the [110] direction of the 48-atom super-cell is the same as the bulk crystal and that of the 96-atom super-cell is twice that of the bulk crystal. The plane-wave cut-off energy is 60 Ryd. We use eight and four special k points in the irreducible fourth of the Brillouin zone for the 48-atom and 96-atom super-cells, respectively. Relaxation is performed according to the Hellmann–Feynman forces. The symmetric property is preserved throughout the relaxation. A spin-unrestricted calculation was performed in this study.

3. Result and discussion

Figure 1 shows the atomic structure of the $(\bar{1}12)$ Σ3 boundary in the [110] projection obtained from the ARHVTEM observation [11, 12]. This boundary structure has no RBT across the $(\bar{1}12)$ boundary plane, which is explained by the CSL theory (CSL model). This type of boundary structure is mainly observed in CVD diamond films [1, 2]. For this CSL model structure, we deal with two models. One is the CSL (1 × 1) model with the same periodicity along the [110] direction as the bulk crystal, and the other is the CSL (1 × 2) model with double periodicity. In the (1 × 2) model, the reconstruction along the [110] direction can be employed to eliminate the dangling bonds at the circled atoms in figure 1. On the other hand,

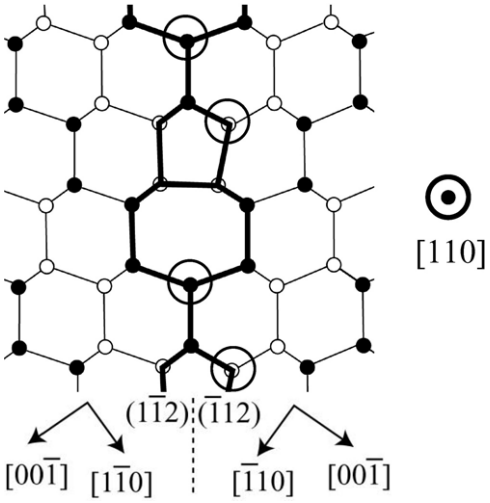

Figure 1. The atomic structure of the ($\bar{1}$12) Σ3 boundary in diamond obtained by ARHVTEM observations [11]. The boundary structure has no rigid-body translation across the ($\bar{1}$12) boundary plane (CSL model). Circles indicate three-fold coordinated atoms in the [110] single-period structure.

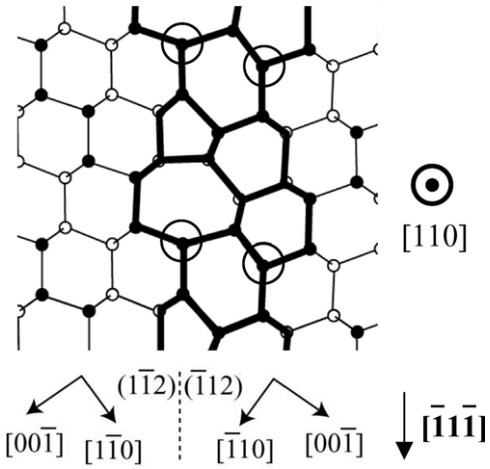

Figure 2. The atomic structure of the ($\bar{1}$12) Σ3 boundary in diamond obtained from ARHVTEM observations [11]. The boundary structure has a rigid-body translation along the [$\bar{1}$1$\bar{1}$] and [$\bar{1}$12] directions across the ($\bar{1}$12) boundary plane (RBT model). Circles indicate three-fold coordinated atoms in the [110] single-period structure.

in the (1 × 1) model, the [110] reconstruction cannot occur, and therefore the circled atoms will remain three-fold coordinated.

The ($\bar{1}$12) Σ3 boundary with the RBT along the [$\bar{1}$1$\bar{1}$] and [$\bar{1}$12] directions is mainly observed in Si and Ge [4, 5], although this type of boundary is occasionally observed in CVD diamond films. Figure 2 shows this structure (RBT model) as also derived from the ARHVTEM observation in diamond [11, 12]. The amount of the RBT is 0.091a_0[$\bar{1}$1$\bar{1}$] and 0.045a_0[$\bar{1}$12], which was measured from the high-resolution images and is consistent with that in Si and

Table 1. The calculated energy of grain boundary (EGB) of the CSL models of the $(\bar{1}12)$ $\Sigma 3$ boundary in diamond.

	(1×1) model	(1×2) model
EGB	6.08 J m^{-2}	5.44 J m^{-2}

Ge [4]. For the RBT model, it is also possible to construct two types of model, the RBT (1×1) and RBT (1×2) models [20].

For these kinds of models in Si, tight-binding calculations by Paxton and Sutton [21] and Kohyama *et al* [22] revealed that the reconstructed bonds along the [110] axis are energetically favourable for making four-coordinated atoms in the (1×2) models. Such reconstructed bonds do not generate any gap states inside the minimum band gap in Si, which is consistent with experimental studies [5]. In the present study, we apply the *ab initio* method to these models in diamond for the first time.

First, we obtained the stable configurations of the CSL models through structural relaxation. The energy values are listed in table 1, where the values of the boundary energy were defined by dividing the increase in energy by the boundary area. The amount of energy increase at boundaries was calculated by subtracting the total energy of the crystal super-cell that had the same number of atoms as the boundary super-cell from the total energy of the boundary super-cell. The energy of the (1×2) model is lower than that of the (1×1) model.

The calculated densities of states (DOS) of the two configurations are shown in figures 3(a) and (b). The DOS of bulk diamond was also calculated by using the 48-atom super-cell for comparison (figure 3(c)). In the (1×1) model, where dangling bonds are not eliminated because of the periodicity, gap states are formed. In the (1×2) model unoccupied gap states are also formed, although the three-fold coordinated atoms have changed into four-fold coordinated atoms through reconstruction. The peaks of the unoccupied gap states are apparently located between the Fermi level and the bulk conduction-band minimum (figure 3(b)).

The CSL (1×2) atomic structure is considered to be a real boundary structure in diamond since its energy is lower than that of the (1×1) model. And this structure should have unoccupied gap states. We have analysed the unoccupied gap states in detail [21, 22]. The charge density distribution of the unoccupied gap state, which was analysed by EELS, can be described using the square of the Kohn–Sham eigenfunction of the unoccupied gap state. The square of the eigenfunction of these unoccupied gap state is shown in figure 4. For the eigenstate at 0.74 eV below the bottom of the bulk conduction band (gap state 1), the wavefunction is mainly localized at atom I (figures 4(a) and (b)). Atom I contributes to the gap states, although it could eliminate the dangling bond with the reconstruction along the [110] axis in the double-period supercell. Figures 4(c) and (d) also show the square of the eigenfunction of the gap state at 0.50 eV below the bottom of the bulk conduction band (gap state 2). The wavefunction is mainly localized at atom II, which also constitutes the reconstructed bond along the $\langle 011 \rangle$ direction.

The reconstructed bonds along the [110] axis in the diamond boundary reveal different features from those of other covalent bonding materials. In order to examine the reconstructed bonds stretched along the [110] axis at atoms I and II, the total valence electron density of the CSL (1×2) model is illustrated in figure 5. Figure 5(a) shows the valence electron density on the (110) plane across atom I, and figure 5(b) shows that of the $(\bar{1}1\bar{1})$ plane. Since the valence electron density becomes high in the three directions around atom I on the (110) plane, atom I has three bonds on this plane. The atom located above atom I along the [110] direction is denoted atom I′. The valence electron density is rather low between atoms I and I′ in figure 5(b).

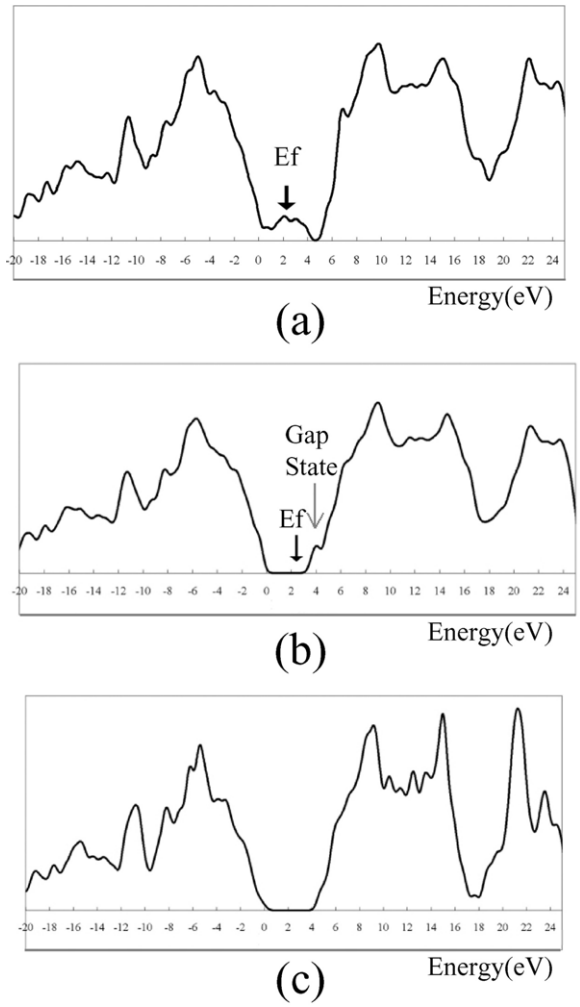

Figure 3. The calculated densities of states for (a) the CSL (1 × 1) model, (b) the CSL (1 × 2) model and (c) the bulk diamond crystal.

The bond length between atoms I and I′ is 115.1% of the bulk diamond bond length. This [110] stretched bond can be regarded as a weak bond. In the same way, figures 5(c) and (d) show the valence electron density on the (110) and $(\bar{1}1\bar{1})$ planes for atom II. Although the valence electron density in the three directions around atom II is sufficiently high on the (110) plane, the density between atoms II and II′ is rather low. The bond length between atoms II and II′ is 112.5% of the bulk diamond bond length, and this [110] stretched bond is also regarded as a weak bond. In the diamond $(\bar{1}12)$ Σ3 boundary, the [110] reconstructed bonds are longer and weaker than the bulk diamond bond. As shown above, the wavefunctions of the unoccupied gap states are mainly localized around the atoms constituting the stretched bonds. Thus, the *ab initio* calculation has shown that the [110] stretched bonds are the origin of the unoccupied gap states in the present diamond boundary.

The RBT models have lower energies than the CSL models and the RBT (1 × 2) model is the most stable, as shown in table 2. The DOSs of the two models are shown in figures 6(a)

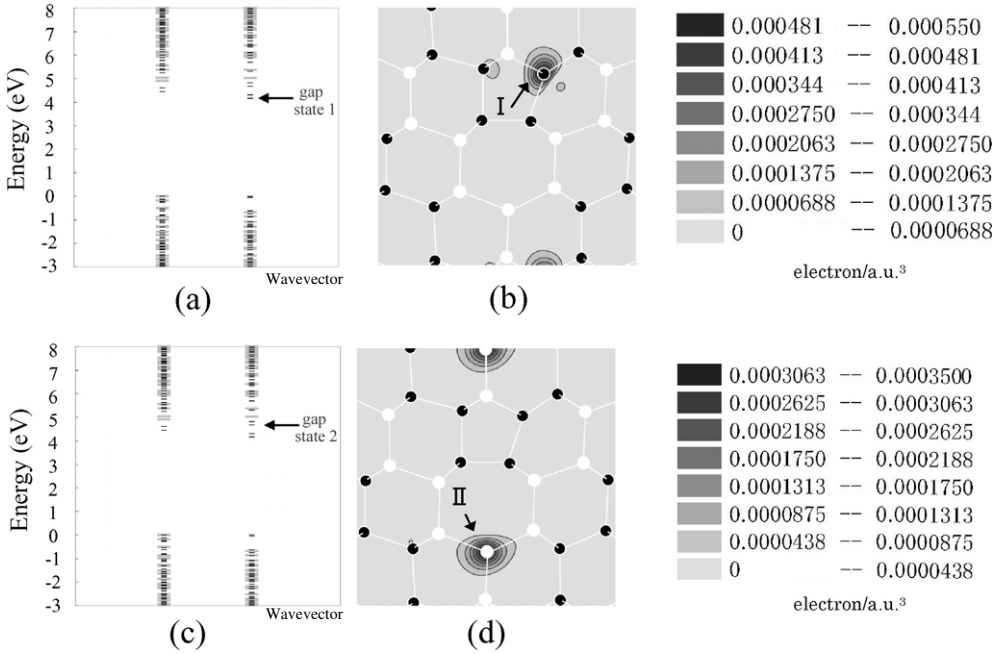

Figure 4. (a) The electronic structure of the CSL (1 × 2) model. Eigenlevels of the 96-atom supercell are plotted for two k points in the Brillouin zone. Grey lines indicate the eigenlevels of the bulk crystal at each k point. The unoccupied gap state at 0.74 eV below the bottom of the bulk conduction band is indicated by an arrow (gap state 1). (b) The square of the eigenfunction of gap state 1. (c) The same as (a), although the unoccupied gap state at 0.50 eV below the bottom of the bulk conduction band is indicated by an arrow (gap state 2). (d) The square of the eigenfunction of gap state 2.

Table 2. The calculated EGB of the RBT models of the $(\bar{1}12)$ $\Sigma 3$ boundary in diamond.

	RBT (1 × 1) model	RBT (1 × 2) model
EGB	3.62 J m^{-2}	2.46 J m^{-2}

and (b). The RBT (1 × 1) model has gap states similar to the CSL (1 × 1) model. On the other hand, the RBT (1 × 2) model has no apparent gap peaks, although the band gap of the RBT (1 × 2) model is slightly narrow due to the boundary states associated with the conduction-band edge, compared to the bulk crystal. These results are similar to the tight-binding calculations of the same RBT models in Si [23, 24], although the RBT (2 × 2) model consistent with the observation in Ge [4] is a little more stable than the (1 × 2) model in Si.

There are bond-length and bond-angle distortions in each reconstructed model. In the RBT (1 × 2) model, the bond-length deviations range from −3.8% to +10.2% and the bond-angle deviations range from −16.9° to +17.0° measured from the tetrahedral angle, while in the CSL (1× 2) model, the bond-length deviations range from −8.3% to +15.1% and the bond-angle deviations range from −29.7° to +23.3°. It can be said that the smaller bond-length and bond-angle deviations of the RBT (1 × 2) model are closely correlated with the relative stability and no apparent gap states.

A correlation exists between the degree of bond distortion and the energy level of the boundary state as previously analysed in Si [25]. In diamond, the [110] bond stretched by

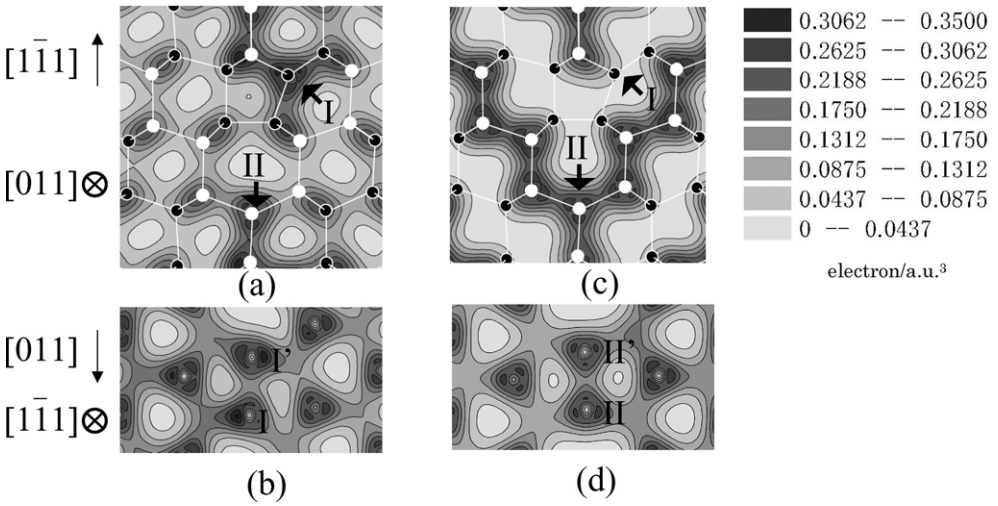

Figure 5. The valence electron density in the CSL (1 × 2) model: (a) the cross-section on the [110] plane containing atom I; (b) the cross-section on the $(\bar{1}1\bar{1})$ plane containing atom I; (c) the cross-section on the [110] plane containing atom II; and (d) the cross-section on the $(\bar{1}1\bar{1})$ plane containing atom II.

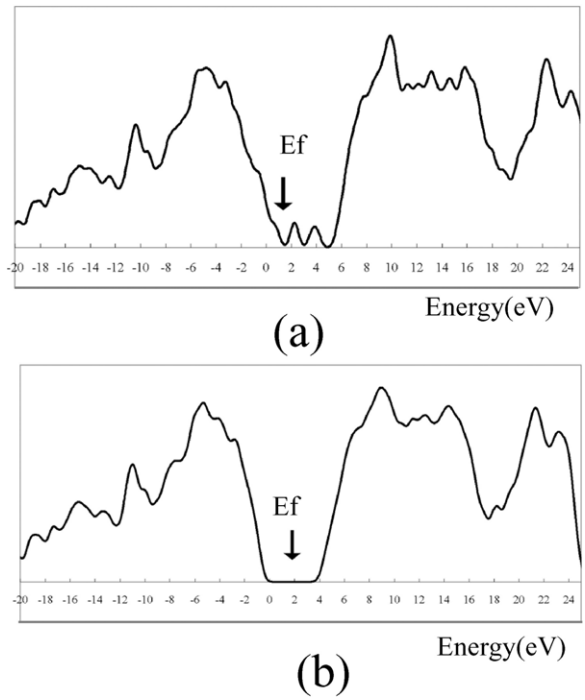

Figure 6. The calculated densities of states for (a) the RBT (1 × 1) model and (b) the RBT (1 × 2) model.

15.1% in the CSL (1 × 2) model causes the gap state at 0.74 eV below the bulk conduction-band minimum, and the [110] bond stretched by 12.5% causes the gap state at 0.50 eV, although

the maximum stretching of 10.2% in the RBT (1×2) model generates no clear gap states except for boundary states associated with the conduction-band edge. Of course, the large bond-angle deviations around the [110] bonds should be also involved in the energy levels of the boundary states of the CSL (1×2) model. The tendency for the boundary states to be generated at the conduction-band edge rather than at the valence-band edge can be explained as follows. Large bond distortions should cause both occupied valence-band edge states and unoccupied conduction-band edge states in the band gap. And occupied valence-band edge states should sink into the bulk valence band through the relaxation, because the relaxation occurs so as to reduce the total energy including occupied valence-band edge states. On the other hand, unoccupied conduction-band edge states tend to remain inside the band gap because they are not directly concerned with total energy or atomic forces.

Finally, the reason why the CSL structure of the {112} $\Sigma 3$ boundary is dominant in diamond in spite of its higher energy, unlike the same type of boundary in Si and Ge, can be explained by the constraint due to the {111} $\Sigma 3$ boundary and the conditions of the CVD process. Among the CSL boundaries, the {111} $\Sigma 3$ boundary is very stable and dominant in number. Other boundaries branch out of the {111} $\Sigma 3$ boundary or their junctions. The $(\bar{1}12)$ $\Sigma 3$ boundary is connected to the $(\bar{1}1\bar{1})$ $\Sigma 3$ boundary at 90°. The $(\bar{1}1\bar{1})$ $\Sigma 3$ boundary has mirror symmetry with respect to the $(\bar{1}1\bar{1})$ plane and does not allow grains across the boundary to translate along $[\bar{1}1\bar{1}]$ or $[\bar{1}12]$ directions. Thus the RBT along the interface for the $(\bar{1}12)$ $\Sigma 3$ boundary should generate substantial strain fields at facets, steps and junctions with the $(\bar{1}1\bar{1})$ $\Sigma 3$ boundary, which should result in significant increases in the strain energy by the high stiffness of diamond. In addition, the lengths of segments of the $(\bar{1}12)$ $\Sigma 3$ boundary sandwiched by the junctions with the $(\bar{1}1\bar{1})$ $\Sigma 3$ boundary in CVD diamond film are relatively short [26], which also makes the CSL structure more favourable because of the relatively severe constraint for the RBT by the $(\bar{1}1\bar{1})$ $\Sigma 3$ boundary, as observed in Au [27] and SiC films [28]. Moreover, the conditions of the CVD process (the temperature involved and the diffusion coefficient at that temperature) used for the formation of diamond films are likely to prevent the atomic structures of grain boundaries from relaxing in a wide range, once the boundary structure is established. Translation, therefore, may not readily occur even when the $(\bar{1}12)$ $\Sigma 3$ boundary becomes long enough for the total energy to be reduced by translation against the strains at the junction. Thus the structure with the RBT should rarely be formed in polycrystalline CVD diamond films.

4. Summary

In summary, the atomic and electronic structure of the $(\bar{1}12)$ $\Sigma 3$ boundary in diamond has been investigated by *ab initio* calculation (density-functional theory with the plane-wave pseudopotential method). The atomic structure models were constructed from the ARHVTEM micrographs. For the CSL structure without the RBT, which is dominant in CVD diamond films due to the constraint of the RBT, unoccupied gap states are observed below the bulk conduction-band minimum, although three-fold coordinated atoms are reconstructed. This is because the [110] reconstructed bonds are largely stretched and can be regarded as weak bonds. These gap states should be the origin of the experimentally observed peak below the σ^* peak in the EELS spectra of this boundary in diamond.

References

[1] Zhang Y, Ichinose H, Nakanose M, Ito K and Ishida Y 1999 *J. Electron Microsc.* **48** 245
[2] Ichinose H and Nakanose M 1998 *Thin Solid Films* **319** 87

[3] Okushi H 2001 *Diamond Relat. Mater.* **10** 281
[4] Bourret A and Bacmann J 1986 *Trans. Japan Inst. Met. Suppl.* **27** 125
[5] Thibault J, Rouviere J L and Bourret A 2000 *Handbook of Semiconductor Technology* vol 1, ed K A Jackson and W Schröter (Weinheim: Wiley–VCH) p 377
[6] Kohyama M 2002 *Modelling Simul. Mater. Sci. Eng.* **10** R31
[7] Kohyama M, Ichinose H, Zhang Y, Ishida Y and Nakanose M 1996 *Mater. Sci. Forum* **207** 265
[8] Morris J R, Fu C L and Ho K M 1996 *Phys. Rev.* B **54** 132
[9] Hohenberg P and Kohn W 1964 *Phys. Rev.* B **136** 864
[10] Kohn W and Sham J L 1965 *Phys. Rev.* **140** A1133
[11] Sawada H and Ichinose H 2001 *Scr. Mater.* **44** 2327
[12] Sawada H, Ichinose H and Kohyama M 2004 *Scr. Mater.* **51** 689
[13] Ichinose H, Sawada H, Takuma E and Osaki E M 1999 *J. Electron Microsc.* **48** 887
[14] Kohyama M 1999 *Phil. Mag. Lett.* **79** 659
[15] Kohyama M 2002 *Phys. Rev.* B **65** 184107
[16] Perdew J P and Zunger A 1981 *Phys. Rev.* B **23** 5048
[17] Troullier N and Martins J L 1991 *Phys. Rev.* B **43** 1993
[18] Payne M C, Teter M P, Allan D C, Arias T A and Joannopoulos J D 1992 *Rev. Mod. Phys.* **64** 1045
[19] Bylander D M, Kleinman L and Lee S 1990 *Phys. Rev.* B **42** 1394
[20] Papon A M and Petit M 1985 *Scr. Metall.* **19** 391
[21] Kohyama M 1997 *Mater. Chem. Phys.* **50** 159
[22] Kohyama M and Takeda S 1999 *Phys. Rev.* B **60** 8075
[23] Paxton A T and Sutton A P 1988 *J. Phys. C: Solid State Phys.* **21** L481
[24] Kohyama M, Yamamoto R, Watanabe Y, Ebata Y and Kinoshita M 1988 *J. Phys. C: Solid State Phys.* **21** L695
[25] Kohyama M and Yamamoto R 1994 *Phys. Rev.* B **50** 8502
[26] Sawada H, Ichinose H, Watanabe H, Takeuchi D and Okushi H 2001 *Diamond Relat. Mater.* **10** 2096
[27] Ichinose H and Ishida Y 1981 *Phil. Mag.* A **43** 1253
[28] Tanaka K and Kohyama M 2002 *Phil. Mag.* A **82** 215